Journal of Advanced Research 39 (2022) 103–117

Contents lists available at ScienceDirect

Journal of Advanced Research

journal homepage: www.elsevier.com/locate/jare

miR-155 down-regulation protects the heart from hypoxic damage by activating fructose metabolism in cardiac fibroblasts

Yu Zhang [a,1], Hong Zhang [a,b,1], Zhan Yang [b], Xin-hua Zhang [a], Qing Miao [c], Min Li [a], Tian-ying Zhai [a], Bin Zheng [a,*], Jin-kun Wen [a,*]

[a] Department of Biochemistry and Molecular Biology, Key Laboratory of Neural and Vascular Biology, Ministry of Education, Hebei Medical University, Shijiazhuang 050017, China
[b] Department of Urology, Second Hospital of Hebei Medical University 050000, China
[c] Department of Cardiovascular Medicine, Second Hospital of Hebei Medical University, 050000, China

HIGHLIGHTS

- miR-155 suppresses splicing factor SKIV2L2 expression by targeting it's 3′ UTR.
- miR-155 deletion enhances SKIV2L2 expression and its interaction with TRA2A.
- SKIV2L2/TRA2A complex suppresses alternative splicing of HIF1α pre-mRNA to form circHIF1α.
- circHIF1α deletion contributes to fructose metabolism by increasing the production of KHK-C.
- Exogenous delivery of SKIV2L2 reduces damage in the infarcted heart.
- miR-155 downregulation protects the heart from hypoxic injury by activating fructose metabolism.

GRAPHICAL ABSTRACT

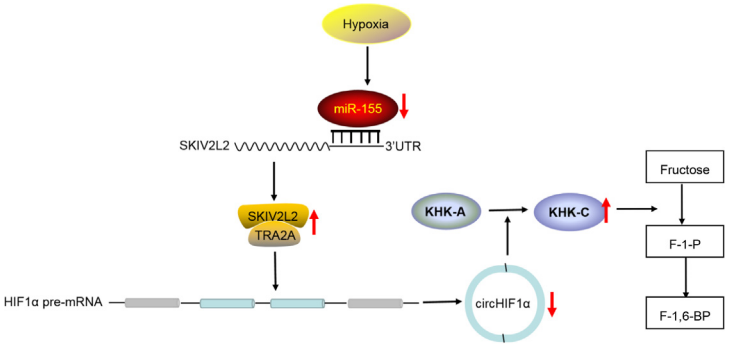

ARTICLE INFO

Article history:
Received 10 August 2021
Revised 15 October 2021
Accepted 17 October 2021
Available online 20 October 2021

Keywords:
MiR-155
Fructose metabolism
KHK-C
CircHIF1α
Alternative splicing

ABSTRACT

Introduction: Hypoxia-inducible factor (HIF)1α has been shown to be activated and induces a glycolytic shift under hypoxic condition, however, little attention was paid to the role of HIF1α-actuated fructolysis in hypoxia-induced heart injury.
Objectives: In this study, we aim to explore the molecular mechanisms of miR-155-mediated fructose metabolism in hypoxic cardiac fibroblasts (CFs).
Methods: Immunostaining, western blot and quantitative real-time reverse transcription PCR (qRT-PCR) were performed to detect the expression of glucose transporter 5 (GLUT5), ketohexokinase (KHK)-A and KHK-C in miR-155$^{-/-}$ and miR-155^{wt} CFs under normoxia or hypoxia. A microarray analysis of circRNAs was performed to identify circHIF1α. Then CoIP, RIP and mass spectrometry analysis were performed and identified SKIV2L2 (MTR4) and transformer 2 alpha (TRA2A), a member of the transformer 2 homolog family. pAd-SKIV2L2 was administrated after coronary artery ligation to investigate whether SKIV2L2 can provide a protective effect on the infarcted heart.

Peer review under responsibility of Cairo University.
* Corresponding authors at: Department of Biochemistry and Molecular Biology, Key Laboratory of Neural and Vascular Biology, Ministry of Education, Hebei Medical University, No. 361 Zhongshan East Road, Shijiazhuang 050017, China.
E-mail addresses: doublezb@hebmu.edu.cn (B. Zheng), wjk@hebmu.edu.cn (J.-k. Wen).
[1] First two authors have contributed equally to the manuscript.

https://doi.org/10.1016/j.jare.2021.10.007
2090-1232/

Results: When both miR-155$^{-/-}$ and miR-155^{wt} CFs were exposed to hypoxia for 24 h, these two cells exhibited an increased glycolysis and decreased glycogen synthesis, and the expression of KHK-A and KHK-C, the central fructose-metabolizing enzyme, was upregulated. Mechanistically, miR-155 deletion in CFs enhanced SKIV2L2 expression and its interaction with TRA2A, which suppresses the alternative splicing of HIF1α pre-mRNA to form circHIF1α, and then decreased circHIF1α contributed to the activation of fructose metabolism through increasing the production of the KHK-C isoform. Finally, exogenous delivery of SKIV2L2 reduced myocardial damage in the infarcted heart.
Conclusion: In this study, we demonstrated that miR-155 deletion facilitates the activation of fructose metabolism in hypoxic CFs through regulating alternative splicing of HIF1α pre-mRNA and thus circHIF1 formation.

Introduction

Ischemic heart disease is the leading cause of death worldwide, which has become a global burden. To maintain the high energy consumption required by pumping oxygenated blood throughout the body, ATP must be continuously synthesized in the heart. In a normal heart, most of the ATP is produced by oxidizing free fatty acids [1]. Upon myocardial ischemia, however, glucose uptake and glycolysis are dramatically increased to ensure sufficient ATP production under hypoxia condition to maintain cardiac function [2]. Under hypoxia stress, hypoxia-inducible factor (HIF)1α is activated to mediate adaptive transcriptional responses to low-oxygen tension and to exert important beneficial roles [2], maintaining cardiomyocyte survival and promoting myocardial angiogenesis and reprogramming of metabolism [3]. On the one hand, HIF1α induces the metabolism from glucose to lactate to provide sufficient energy and glycolytic intermediates that support biosynthesis in hypoxia-induced cardiac hypertrophy. On the other hand, HIF1α actuates fructose metabolism by acting as a major regulator of the alternative splicing machinery, transcriptionally activating a number of splicing factors [4]. Mechanistic studies have shown that HIF1α activates fructolysis via facilitating SF3B1 binding to fructose-metabolizing enzyme (ketohexokinase, KHK) pre-mRNA, which contributes to the alternative splicing of KHK pre-mRNA to generate KHK-C isoform, an active form of KHK. Under hypoxia, induction of HIF1α leads to increased binding of SF3B1 to the branch point ahead of KHK exon 3c, resulting in the production of the KHK-C isoform [2,4] and thus enforcing fructolysis and inducing pathological cardiac hypertrophy [4]. Despite increased knowledge of the metabolic alterations that occur in hypoxic myocardial tissue, the molecular mechanisms linking HIF1α to fructose metabolism in hypoxic cardiac fibroblasts (CFs) remain poorly understood. Significance of fructolysis in hypoxic CFs is also unclear.

Accumulating evidence suggests that hypoxic modulation of cell function can be mediated by microRNAs (miRs), which are single-stranded noncoding RNAs of 22–25 nucleotides. miR-155 is a multifunctional microRNA and is critical for various physiological and pathological processes including inflammation, differentiation, proliferation, oxidative stress, and cardiovascular remodeling [5,6]. Several studies have shown that HIF1α upregulates miR-155 expression in human cancer by direct binding to hypoxia response elements on the miR-155 promoter [7,8], and in turn, miR-155 suppresses HIF1α expression via targeting it's 3′ untranslated region, forming a HIF1α-miR-155 negative feedback loop to maintain the oxygen homeostasis, and thus leading to oscillatory behavior of HIF1α-dependent transcription [8]. Our previous studies revealed that a positive feedback loop between TNF-α and miR-155 can be formed in macrophages, which participates in the process of atherosclerosis [9], and that miR-155 mediates the activation of p47^{phox} and NF-κB by MST2 and integrates inflammation and oxidative stress, which cooperatively promotes vascular smooth muscle cell (VSMC) proliferation, migration and vascular remodeling [5]. These observations suggest that miR-155 is an important mediator of cardiovascular disease, and that its dysregulation might be implicated in hypoxia-induced heart injury. However, it remains unknown whether miR-155 participates in hypoxia-induced metabolic alterations in CFs, and what mechanisms are involved in this process?

In this study, we investigated whether and how miR-155 deletion facilitates the activation of fructose metabolism in hypoxic CFs through regulating alternative splicing of HIF1α pre-mRNA and thus circHIF1α formation.

Materials and methods

Ethics statement

All procedures involving experimental animals were performed in accordance with the principles and guidelines established by the National Institute of Medical Research (INSERM) and were approved by the local Animal Care and Use Committee. The investigation conforms to the directive 2010/63/EU of the European parliament.

Animals and treatment

miR-155$^{-/-}$ and SKIV2L2$^{-/-}$ mice were purchased from Jackson Laboratory (Bar Harbor, ME, USA). C57BL/6J mice were obtained from Vital River Laboratory Animal Technology Co., Ltd. (Bejing, China). Mice were fed in a SPF-rated animal house at Hebei Medical University and housed on a 12-hour light–dark cycle (7:00 am to 7:00 pm, light). Mice used for experiments were adult mice over 8 weeks of age. In vivo, a mouse myocardical infraction (MI) model (n = 5 mice/group) was established by ligating the left coronary artery, and adenovirus (pAd-GFP or pAd-SKIV2L2, 10^9 PFU/ml, 50 ul/mouse) was injected at multiple points in the ischemic area at the same time.

Cell culture and transfection

Primary CFs were isolated from the P1–P3 newborn mice [10]. Briefly, mouse heart was removed and dissected rapidly. Then the tissues were washed with cold PBS for 3 times and digested using 0.25 % Trypsin-EDTA Solution at 4 °C overnight to hydrolyze extracellular matrix. Next day, the heart fragments were retrieved and incubated with digestion buffer (complete culture medium + 0.5 mg/ml-1.0 mg/ml collagenase II + 5 mg/ml albumin) at 37 °C for several times in a short time. After digestion, cell suspension was subjected to centrifugation at 1000 × g for 5 min. 1 × 10^6 cells were seeded in culture plates. After 60 min, changed the culture medium in order to remove unattached cardiomyocytes. The second and third generation CFs were used for experiments. All the cells were cultured in DMEM/F12 medium with 10% fetal bovine serum (FBS) at 37 °C and 5% CO_2. For hypoxia conditions, cells were cultured

at 37 °C in the presence of 5% CO_2 and 1% O_2. Lipofectamine 2000 (Invitrogen) and miR-155 inhibitor/inhibitor NC or siRNA (si-SKIV2L2, si-TRA2A) were used for transfection [11]. Cells were harvested and analyzed 24 h after transfection.

Adenoviral vectors

pAd-GFP and pAd-SKIV2L2 were constructed by Shanghai Hanheng Biotechnology company. Cells were allowed to grow in complete medium to 70% density and cultured for 24 h without FBS. Then virus infection was performed.

Analysis of stained sections

Formalin-fixed, paraffin-embedded myocardial specimens were sectioned at 4 μm and analyzed by hematoxylin/eosin (HE) staining for morphology. The sections were visualized using a Leica light microscope (Leica Microsystems Gmbh, Wetzlar, Germany). A minimum of 8 mice per genotype was analyzed for the morphometric measurements. Protein expression and distribution were detected by Immunofluorescence. The antibodies used included monoclonal anti-CD34 (1:50; ab81289, Abcam) and monoclonal anti-CD31 (1:50; ab281583, Abcam).

RNA isolation, reverse transcription and real-time PCR

The total RNA from the miR-155$^{-/-}$ or miR-155^{wt} CFs [12] was isolated using RNeasy Micro Kit (QIAGEN, Germany). The RNA purity and concentration were assessed in an UV spectrophotometer (Thermo). Reverse transcription was performed with the RevertAid First Strand cDNA Synthesis Kit (K1622, Thermo Fisher Scientific-CN) according to the manufacturers' procedure. miRNA was extracted using the miRNeasy Mini Kit (Qiagen, ON, Canada) and reverse-transcribed with the RT2 miRNA First Strand Kit (Qiagen, ON, Canada) according to the manufacturers' instructions. Primers used in this study are listed in Table S3.

Cell viability assay

The cell viability was evaluated by CCK-8, as described previously [13]. In brief, 1×10^4 CFs/well were seeded in triplicate into 96-well plates and incubated overnight. After treatment, the CCK-8 working solution (10 μL) was added to the wells, and the plates were then incubated for 2 h at 37 °C. The absorbance was measured in a Thermo Fluoroscan Ascent spectrometer at 450 nm. Results were shown as the mean ± SEM of absorbance relative to time 0 or control.

Western blotting

Proteins were extracted from CFs as previously described [14], and then separated by sodium dodecyl sulfate–polyacrylamide gel electrophoresis (SDS-PAGE). The separated proteins were transferred from the gel onto polyvinylidene difluoride membranes. Membranes were incubated with 5% milk for 2 h at 37 °C and overnight at 4 °C with primary antibodies: GLUT5 antibody (1:1000, 27571–1-AP, Proteintech), GLUT1 antibody (1:1000, ab115730, Abcam), HIF1α antibody (1:1000, ab179483, Abcam), SKIV2L2 antibody (1:1000, ab70551, Abcam), TRA2A antibody (1:100, ab169052, Abcam), GAPDH antibody (1:1000, Santa Cruz, USA) and β-actin antibody (1:5000, Santa Cruz, USA). The membranes were then incubated for 1 h at room temperature with the corresponding secondary antibodies (1:2000, CST, USA). Immunoreactive bands were tested by chemiluminescence (ECL reagents, Millipore, Massachusetts, USA) and exposed to an X-ray film for densitometric analysis.

Immunofluorescence

CFs were seeded in 6-well plates, cultured overnight and treated with or without miR-155 inhibitors or mimics. Then cells were washed with cold 1 × PBS, fixed with 4% paraformaldehyde for 10 min at room temperature, after blocking with 10% goat serum, they were incubated with the primary antibodies at 4 °C overnight and then probed with Alexa Fluor-conjugated secondary antibodies. Fluorescence images of the cells were captured using Confocal microscope [15].

Luciferase assay (3′-UTR reporter assays)

CFs were transfected with 100 pmol of pre-miR-Ctrl or pre-miR-155 and 1 μg of psiCHECK2 vector (Promega) expressing the 3′-UTR of the SKIV2L2 mRNA or the mutated 3′-UTR of the SKIV2L2 mRNA. After 24 h, the luciferase activity was tested using the Dual-Luciferase Reporter Assay System (Promega).

2-NBDG assay

CFs were seeded in 96-well plates and incubated at 37 °C for the different times. Each group consisted of 6 subsidiary pores. After incubation for 24 h, the cell density grew to about 90%, and 2-[N-(7-nitrobenz-2-oxa-1,3-diazol-4-yl) amino]-2-deoxy-D-glucose (2-NBDG) (Life Technologies) with final concentration of 100 μm/L was added. After incubation at 37 °C for 20 min, washed the cells with PBS solution 3 times, and then added 100 μL of PBS solution into each pore. Cells were observed and photographed by fluorescence microscope [16].

Affinity purification with biotinylated nucleotide (Oligo pull down)

CFs were collected after appropriate stimulation for 24 h. Cell lysis was performed by adding 1 mL of lysis solution (50 mM Tris, 10 mM EDTA, 5 mM NaF, 1% SDS, 1 mM DTT, 150 mM NaCl, and protease and phosphatase inhibitors) to the collected cells. Then 2 mL of hybridization buffer (1 mM DTT, 1 mM EDTA, 1% SDS, 5 mM NaF, 50 mM Tris, 750 mM NaCl, and phosphatase and protease inhibitors) was added. The mixture was incubated with streptavidin-agarose beads for 30 min at 37 °C. The lysates were separated from the beads by a magnetic holder. The presence of SKIV2L2 binding was detected by Western blot [15].

Periodic acid schiff (PAS) staining

The cells were fixed by 4% paraformaldehyde, stained by PAS according to the manufacturer's protocols (Solarbio, G1280) and then observed under a light microscope (Leica DFC 310) [17].

RNA immunoprecipitation (RIP)

CFs were cross-linked by adding 10% formaldehyde solution and shaken slowly for 10 min at room temperature. Added 10 times the volume of 2.66 M glycine to the cross-linking system, leave it at room temperature for 5 min and ice bath for 10 min, then collected the cells and performed lysis. The supernatant was added to the protein-A/G magnetic bead mixture coated with antibodies and incubated for 4 h at room temperature or overnight at 4 °C. Added 1 mL of pre-cooled IP buffer (150 mM NaCl, 10 mM Tris-HCl (pH 7.4), 1 mM EDTA, 1 mM EGTA (pH 8), 1 % Triton X-100, 0.5% NP-40, 1 mM DTT, 200 units/ml RNase OUT, EDTA-free protease inhibitor Cocktail), and mixed with strong shaking. After a short centrifugation, the sample was shaken to the bottom of the tube, placed on a magnetic holder in an ice bath, and the supernatant was discarded after 1 min, and repeated 5 times. The precipitate

was the sample obtained from the RIP experiment, which can be further digested by proteinase K to extract RNA for subsequent analysis. The RNA enrichment was assessed by RT-qPCR. Primers used in this study are listed in Table S2 [18].

Lactic acid and pyruvic acid assay

Lactic acid and pyruvic acid were determined by derivatization USAEME-GC. The specific steps were as follows: 2×10^5 cells were seeded in 6-well plates and treated for 24 h. Then the cell culture media were diluted with deionized water 4 times. The treated samples were mixed with methoxyamine hydrochloride solution and incubated at 60 °C for 5 min. Then, a mixture of isobutyl chloroformate and carbon tetrachloride was rapidly injected followed by vigorous shaking and ultrasonic treatment. After centrifugation, 1 μL of carbon tetrachloride layer was injected for analysis by GC-FID [19].

Statistical analysis

Statistical analyses were performed by Student *t*-test and one-way ANOVA. Differences between the mean values were analyzed using Bonferroni post hoc tests or a Mann-Whitney *U* test (non-parametric). The data are presented as the mean ± SEM. $P < 0.05$ was considered statistically signifificant. $P > 0.05$ means no statistical significance.

Results

miR-155 downregulation enhances fructose metabolism in hypoxia-exposed CFs

miR-155 is a multifunctional microRNA that is implicated in hypoxia-induced heart injury [20,21] and we found that miR-155 gene knockout (miR-155$^{-/-}$) mice exhibited a stronger anti-hypoxia ability than miR-155^{wt} mice, showing that the survival time of miR-155$^{-/-}$ mice was much longer than that of miR-155^{wt} mice after acute hypoxia (Supplemental data, SFig.1). Therefore, we sought to determine the relationship between miR-155 expression and hypoxia exposure in CFs. The results showed that the expression level of miR-155 was gradually decreased with the prolongation of hypoxia time (Fig. 1A). Next, we isolated CFs from miR-155$^{-/-}$ and miR-155^{wt} mice and confirmed a significantly lower expression of miR-155 in CFs from miR-155$^{-/-}$ mice (thereafter known as miR-155$^{-/-}$ CF) than those from miR-155^{wt} mice (thereafter known as miR-155^{wt} CF) (Supplemental data, SFig. 2A). We found that the cell viability of miR-155$^{-/-}$ CFs was significantly enhanced upon exposure to hypoxia for 24 and 48 h relative to that of miR-155^{wt} CFs (Fig. 1B). We then examined the effect of hypoxia on glucose metabolism and found that in miR-155$^{-/-}$ CFs vs. miR-155^{wt} CFs, the hypoxia caused an increased glucose uptake into CFs (Fig. 1C), a decreased level of intracellular glycogen content (Fig. 1D) as well as a trend for increased expression of the major genes involved in glycolysis, such as pyruvate dehydrogenase kinase isozyme 1 (PDK1) [22,23], M2 pyruvate kinase (PKM2) [24], triokinase and hexokinase (Fig. 1E). However, the knockout of miR-155 in CFs had little effect on uncoupling protein 2 (UCP2) and acyl-coenzyme aoxidase 1 (ACOX1), the major genes of fatty acid metabolism. UCP2 is a protein critical for supporting fatty acid oxidation and acts as a critical regulator of glucose-dependent de novo lipid synthesis [25,26]. ACOX1 is another key enzyme of the fatty acid oxidation pathway [27,28], which catalyzes the first step of peroxisomal β-oxidation, desaturating acyl-CoA to 2-*trans*-enoyl-CoA (Supplemental data, SFig. 2B). At the same time, increased contents of lactate and pyruvate were observed in the culture media of miR-155$^{-/-}$ CFs vs. miR-155^{wt} CFs regardless of treatment with hypoxia. Moreover, hypoxia further increased the content of these two metabolites in miR-155$^{-/-}$ CFs (Fig. 1F, G), suggesting that the absence of miR-155 facilitates glycolysis in hypoxia-exposed CFs. Accordingly, the extracellular acidification rate (ECAR) was significantly increased in miR-155$^{-/-}$ CFs relative to miR-155^{wt} CFs under hypoxia (Fig. 1H), reflecting a compromised energy metabolism in miR-155$^{-/-}$ CFs.

To explore how miR-155 affects glucose metabolism under hypoxia, we examined the expression of some genes related to glucose transport. As shown in Fig. 1I and J, the exposure of miR-155$^{-/-}$ and miR-155^{wt} CFs to hypoxia markedly increased GLUT1 protein and mRNA expression levels. Interestingly, the expression of GLUT5 mRNA and protein, a fructose transporter, was significantly upregulated in miR-155$^{-/-}$ CFs (Fig. 1I, J). Further studies showed that mRNA expression level of the fructose metabolism-related ketohexokinase-A (KHK-A) and its active form ketohexokinase-C (KHK-C) was significantly increased only in miR-155$^{-/-}$ CFs exposed to hypoxia (Fig. 1K), while an increased protein level of KHK-C seems to be related to both hypoxia and deletion of miR-155 in CFs (Fig. 1L). These results suggest that miR-155 deletion in CFs facilitates the activation of KHK-A by hypoxia, indicating that besides increasing glycolysis, hypoxia could possibly trigger fructose metabolism in miR-155$^{-/-}$ CFs.

The absence of miR-155 in CFs actuates fructose metabolism by inducing circHIF1α and thus KHK-C generation

To dissect the molecular mechanism whereby miR-155 downregulation triggers frutcose metabolism in CFs under hypoxia, we performed a microarray analysis of circRNAs in miR-155$^{-/-}$ vs. miR-155^{wt} CFs exposed to hypoxia for 24 h. As a result, 5991 circRNAs were shown to be differentially expressed in these two cells (ANOVA, $p < 0.05$). In addition, 112 of these circRNAs were downregulated (>2-fold) and 270 were upregulated (<−2-fold) (Fig. 2A;

Fig. 1. miR-155 downregulation enhances fructose metabolism in hypoxia-exposed CFs. (A) CFs were exposed to hypoxia for different times. miR-155 expression was detected by qRT-PCR. ***P < 0.001 vs. 0 h. (B) The cell viability of miR-155$^{-/-}$ and miR-155^{wt} CFs exposed to hypoxia for 24 and 48 h was detected using CCK-8. **P < 0.01 vs. miR-155^{wt} (C) Glucose uptake was detected using 2-NBDG in a final concentration of 100 μM. Cells were observed and photographed by fluorescence microscope. **P < 0.01 vs. miR-155^{wt} (D) Glycogen content was detected with periodic acid-Schiff (PAS) staining in miR-155$^{-/-}$ and miR-155^{wt} CFs exposed to hypoxia for 24 h. Representative images (left) and semi-quantitative chart (right). ***P < 0.001 vs. miR-155^{wt} (E) The expression of PDK1, PKM2, triokinase and hexokinase was detected using qRT-PCR in miR-155$^{-/-}$ or miR-155^{wt} CFs exposed to hypoxia for 24 h. *P < 0.05 vs. miR-155^{wt} (F) The lactic acid in the culture medium of miR-155$^{-/-}$ or miR-155^{wt} CFs was detected by derivatization USAEME-GC after exposure to normoxia or hypoxia for 24 h. **P < 0.01 and ***P < 0.001 vs. their corresponding control. (G) The pyruvic acid in the culture medium of miR-155$^{-/-}$ or miR-155^{wt} CFs was detected by derivatization USAEME-GC after exposure to normoxia or hypoxia for 24 h. **P < 0.01 vs. their corresponding control. (H) Raw traces of extracellular acidification in miR-155$^{-/-}$ and miR-155^{wt} CFs exposed to hypoxia for 24 h. ***P < 0.001 vs. miR-155^{wt} (I) GLUT1, GLUT5 and HIF1α expression was detected by Western blot in miR-155$^{-/-}$ or miR-155^{wt} CFs exposed to normoxia or hypoxia for 24 h. Representative images (left) and semi-quantitative chart (right). *P < 0.05, **P < 0.01 and ***P < 0.001 vs. miR-155^{wt} (J) GLUT1 and GLUT5 mRNA was detected by qRT-PCR in miR-155$^{-/-}$ and miR-155^{wt} CFs treated as in (I). *P < 0.05 vs. miR-155^{wt} + hypoxia. (K) miR-155$^{-/-}$ and miR-155^{wt} CFs were treated as in (I), KHK-A and KHK-C mRNA was detected by qRT-PCR. *P < 0.05 and **P < 0.01 vs. miR-155^{wt} + hypoxia. (L) miR-155$^{-/-}$ and miR-155^{wt} CFs were treated as in (I), KHK-A and KHK-C protein was detected by Western blot. Representative images (left) and semi-quantitative chart (right). The data are expressed as the mean ± SEM of three independent experiments. *P < 0.05 and **P < 0.01 vs. miR-155^{wt}.

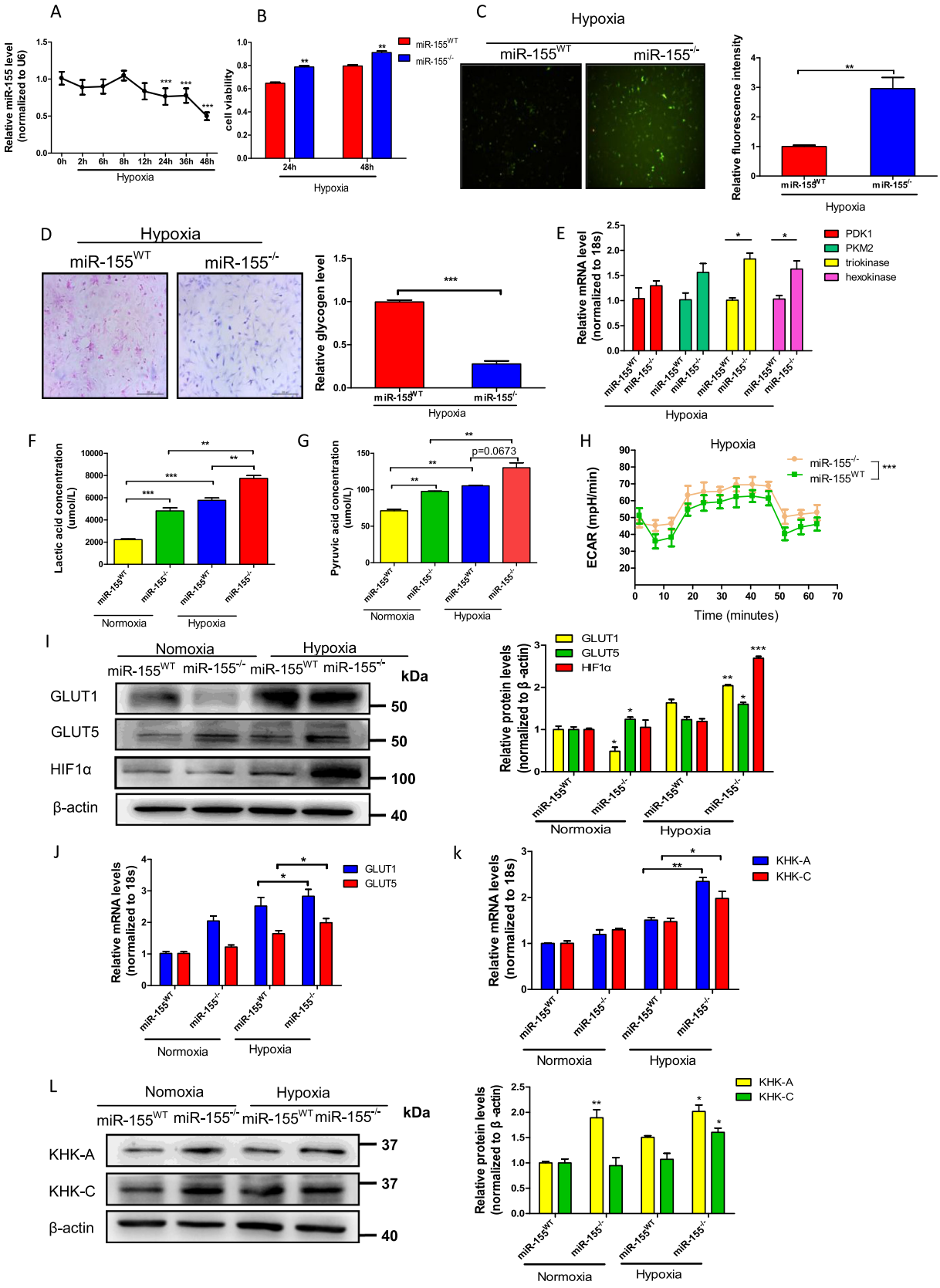
A
Relative miR-155 level (normalized to U6)
0h 2h 6h 8h 12h 24h 36h 48h
Hypoxia
B
cell viability
miR-155WT
miR-155-/-
24h 48h
Hypoxia
C
Hypoxia
miR-155WT
miR-155-/-
Relative fluorescence intensity
Hypoxia
D
Hypoxia
miR-155WT
miR-155-/-
Relative glycogen level
Hypoxia
E
Relative mRNA level (normalized to 18s)
PDK1
PKM2
triokinase
hexokinase
Hypoxia
F
Lactic acid concentration (umol/L)
Normoxia
Hypoxia
G
Pyruvic acid concentration (umol/L)
p=0.0673
Normoxia
Hypoxia
H
Hypoxia
ECAR (mpH/min)
miR-155-/-
miR-155WT
Time (minutes)
I
Nomoxia
Hypoxia
miR-155WT miR-155-/- miR-155WT miR-155-/-
kDa
GLUT1
GLUT5
HIF1α
β-actin
50
50
100
40
Relative protein levels (normalized to β -actin)
GLUT1
GLUT5
HIF1α
Normoxia
Hypoxia
J
Relative mRNA levels (normalized to 18s)
GLUT1
GLUT5
Normoxia
Hypoxia
k
Relative mRNA levels (normalized to 18s)
KHK-A
KHK-C
Normoxia
Hypoxia
L
Nomoxia
Hypoxia
miR-155WT miR-155-/- miR-155WT miR-155-/-
kDa
KHK-A
KHK-C
β-actin
37
37
40
Relative protein levels (normalized to β -actin)
KHK-A
KHK-C
Normoxia
Hypoxia

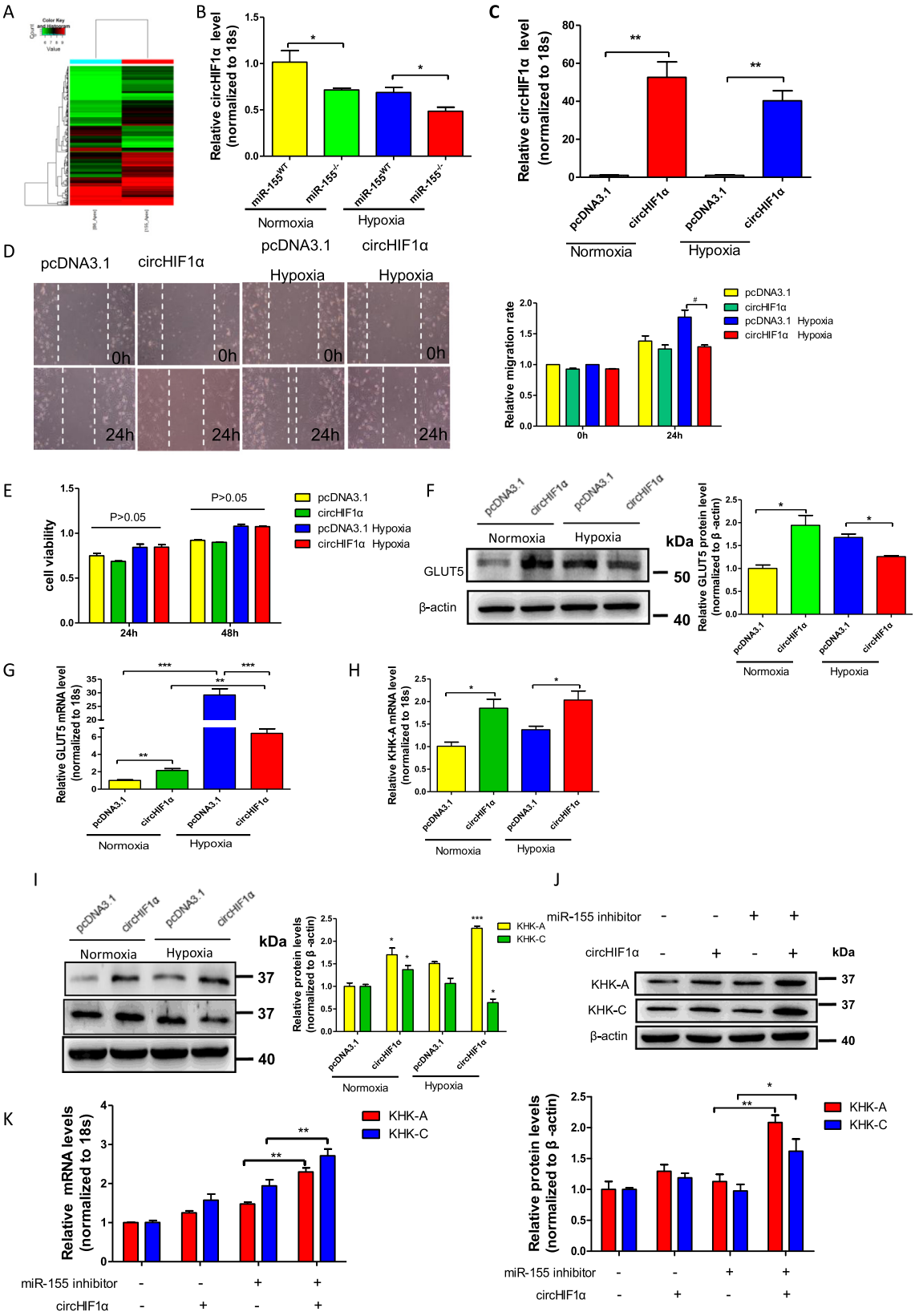
A
B
Relative circHIF1α level (normalized to 18s)
miR-155WT
miR-155-/-
Normoxia
Hypoxia
C
Relative circHIF1α level (normalized to 18s)
pcDNA3.1
circHIF1α
D
pcDNA3.1
circHIF1α
Hypoxia
0h
24h
Relative migration rate
E
cell viability
P>0.05
24h
48h
F
GLUT5
β-actin
kDa
Relative GLUT5 protein level (normalized to β -actin)
G
Relative GLUT5 mRNA level (normalized to 18s)
H
Relative KHK-A mRNA level (normalized to 18s)
I
KHK-A
KHK-C
Relative protein levels (normalized to β -actin)
J
miR-155 inhibitor
circHIF1α
K
Relative mRNA levels (normalized to 18s)
Relative protein levels (normalized to β -actin)

Fig. 2. miR-155 downregulation in CFs induces circHIF1α and thus KHK-C generation. (A) Microarray analysis of circRNAs in miR-155$^{-/-}$ vs. miR-155^{wt} CFs exposed to hypoxia for 24 h. (B) circHIF1α expression was detected by qRT-PCR in miR-155$^{-/-}$ and miR-155^{wt} CFs exposed to normoxia or hypoxia for 24 h. *P < 0.05 vs. miR-155^{wt} (C) circHIF1α expression in CFs transfected with circHIF1α expression vector was detected using qRT-PCR. **P < 0.01 vs. pcDNA3.1. (D) CF migration was detected by wound-healing assay immediately after scratching and at 24 h later. Representative photomicrographs (left), Quantification of cells migrating into the scratch gap (right). #P < 0.05 vs. pcDNA3.1 + hypoxia. (E) CFs were transfected with circHIF1α expression vector and then exposed to hypoxia for 24 and 48 h. The cell viability was detected using CCK-8. (F) CFs were transfected with circHIF1α expression vector and then exposed to normoxia or hypoxia for 24 h. GLUT5 expression was detected by Western blot. Representative images (left) and semi-quantitative chart (right). *P < 0.05 vs. pcDNA3.1. (G) GLUT5 mRNA expression in CFs treated as in (F) was detected using qRT-PCR. **P < 0.01 and ***P < 0.001 vs. their corresponding control. (H) KHK-A mRNA expression in CFs treated as in (F) was detected using qRT-PCR. *P < 0.05 vs. pcDNA3.1. (I) KHK-A and KHK-C expression in CFs treated as in (F) was detected using Western blot. Representative images (left) and semi-quantitative chart (right). *P < 0.05 and ***P < 0.001 vs. pcDNA3.1. (J, K) CFs were transfected with circHIF1α expression vector and miR-155 inhibitor either alone or together, and then KHK-A and KHK-C protein (J) and mRNA (K) expression was detected using Western blot and qRT-PCR, respectively. *P < 0.05 and **P < 0.01 vs. miR-155 inhibitor. The results in (A)–(K) are mean ± SEM from 3 independent experiments.

Supplemental data, Table S1). Among the downregulated circRNAs, circHIF1α, a circRNA derived from hypoxia-inducible factor 1α (HIF1α), has attracted our attention. We further validated a significant decrease of circHIF1α in miR-155$^{-/-}$ CFs exposed to hypoxia for 24 h (Fig. 2B). Sequence analysis showed that circHIF1α is generated from exon 2 and exon 8 of HIF1α gene by back-splicing. Considering that miR-155 regulates the expression of HIF1α [29] and that myocardial hypoxia actuates fructose metabolism through HIF1α activation of SF3B1 and SF3B1-mediated splice switching of KHK-A to KHK-C [4], we investigated whether the downregulation of circHIF1α by miR-155 depletion is responsible for hypoxia-activated fructose metabolism. To do this, we constructed the expression vector of circHIF1α and confirmed its successful expression in CFs regardless of treatment with hypoxia (Fig. 2C). Overexpression of circHIF1α obviously inhibited the migration of CFs induced by hypoxia (Fig. 2D), but had little effect on the proliferation of CFs (Fig. 2E). Simultaneously, circHIF1α overexpression downregulated GLUT5 mRNA and protein levels (Fig. 2F, G) as well as KHK-C protein level (Fig. 2I) in CFs exposed to hypoxia. Reversely, under normoxia, its overexpression significantly increased the expression levels of GLUT5 protein (Fig. 2F) and mRNA (Fig. 2G), KHK-A mRNA (Fig. 2H) and protein (Fig. 2I) as well as KHK-C protein (Fig. 2I). These results suggest that circHIF1α-mediated regulation of fructose metabolism in CFs is different between normoxia and hypoxia.

To provide additional evidence that miR-155 depletion in CFs triggers fructose metabolism under hypoxia by inducing circHIF1α formation, we performed another experiment in which miR-155 was silenced by its antagomir in circHIF1α-overexpressing CFs (Supplemental data, SFig. 3A). As shown in Fig. 2J and K, combining circHIF1α overexpression with miR-155 silencing significantly enhanced the expression of fructose-metabolizing enzymes KHK-A and KHK-C in CFs. These results further suggest that decreased expression of circHIF1α by miR-155 downregulation contributes to the activation of fructose metabolism through inducing production of the KHK-C isoform.

miR-155 targets SKIV2L2 that regulates GLUT5 and KHK-A expression

To investigate how miR-155 regulates circHIF1α formation, we carried out RNA pull-down and mass spectrometry analysis to screen circHIF1α-interacting proteins that are differentially expressed in miR-155$^{-/-}$ and miR-155^{wt} CFs under hypoxia. As a result, 590 RNA binding proteins (RBPs) were identified to be significantly different between these two cells (ANOVA, p < 0.01). Among them, 16 RBPs were identified to be participated in RNA splicing regulation, including circRNA stability, reverse splicing, translation and circRNA export. Among these candidates, we focused on SKIV2L2 (also named as MTR4), an ATP-dependent RNA helicase [30] that is involved in pre-mRNA splicing. Our study showed that knockout of miR-155 in CFs significantly elevated the expression of SKIV2L2 mRNA (Fig. 3A) and protein (Fig. 3B) regardless of hypoxia treatment. To identify whether SKIV2L2 affects fructose metabolism, we constructed adenovirus-mediated SKIV2L2 expression vector and verified its successful overexpression in CFs (Supplemental data, SFig. 3B). Overexpression of SKIV2L2 substantially increased the expression of GLUT5 and KHK-A, but had little effect on glucose transporter GLUT1 (Fig. 3C) and lactic acid concentration regardless of treatment with hypoxia (Fig. 3D). On the contrary, knockdown of SKIV2L2 (Fig. 3E) in hypoxia-exposed CFs by siRNA decreased the expression of GLUT5 and KHK-A protein (Fig. 3F), demonstrating that SKIV2L2 may be implicated in the regulation of GLUT5 and KHK-A expression and subsequent switch to fructose metabolism in CFs.

To further understand the actual relationship between SKIV2L2 and miR-155, bioinformatics analysis was performed and identified that SKIV2L2 harbors a conserved binding site for miR-155 within its 3′ untranslated region (3′ UTR). Reporter gene assay showed that miR-155 significantly downregulated luciferase activity driven by SKIV2L2 3′ UTR (Fig. 3G). These findings indicated that increased SKIV2L2 by miR-155 downregulation facilitates GLUT5 and KHK-A expression probably through inducing circHIF1α formation, which in turn actuates fructose metabolism.

SKIV2L2 mediates miR-155 regulation of circHIF1α expression

To investigate how SKIV2L2 regulates circHIF1α formation, adenovirus-mediated SKIV2L2 transfection was performed, and the results showed that overexpression of SKIV2L2 decreased circHIF1α biogenesis under hypoxia (Fig. 4A), whereas siRNA-mediated knockdown of SKIV2L2 facilitated circHIF1α expression compared with those transfected with control siRNA (si-con) (Fig. 4B). To examine the specificity of SKIV2L2-regulated circHIF1α expression, we detected the effect of SKIV2L2

Fig. 3. miR-155 targets SKIV2L2 that regulates GLUT5 and KHK-A expression. (A) SKIV2L2 mRNA expression was detected by qRT-PCR in miR-155$^{-/-}$ and miR-155^{wt} CFs exposed to hypoxia for 24 h. *P < 0.05 vs. miR-155^{wt} (B) SKIV2L2 protein expression in miR-155$^{-/-}$ and miR-155^{wt} CFs exposed to hypoxia for 24 h was detected by Western blot. Representative images (left) and semi-quantitative chart (right). *P < 0.05 vs. miR-155^{wt} (C) CFs were transfected with pAd-SKIV2L2 and then exposed to normoxia or hypoxia for 24 h. GLUT1, GLUT5 and KHK-A expression was detected by Western blot. Representative images (left) and semi-quantitative chart (right). *P < 0.05, **P < 0.01 and ***P < 0.001 vs. pAd. (D) CFs were treated as in (C), the lactic acid in the culture medium was detected by derivatization USAEME-GC. (E) CFs were transfected with si-SKIV2L2 and then exposed to normoxia or hypoxia for 24 h. SKIV2L2 mRNA expression was detected by qRT-PCR. *P < 0.05 vs. si-con. (F) CFs were transfected with si-SKIV2L2 and then exposed to hypoxia for 24 h. SKIV2L2, GLUT5 and KHK-A expression was detected by Western blot. Representative images (left) and semi-quantitative chart (right). *P < 0.05 and **P < 0.01 vs. si-con. (G) Luciferase reporter assays were performed in CFs co-transfected with SKIV2L2 3′ UTR-luciferase reporter and miR-155 mimic or miR-155 inhibitor. *P < 0.05 vs. NC mimic. Data in (A)-(G) are mean ± SEM from 3 to 5 independent experiments.

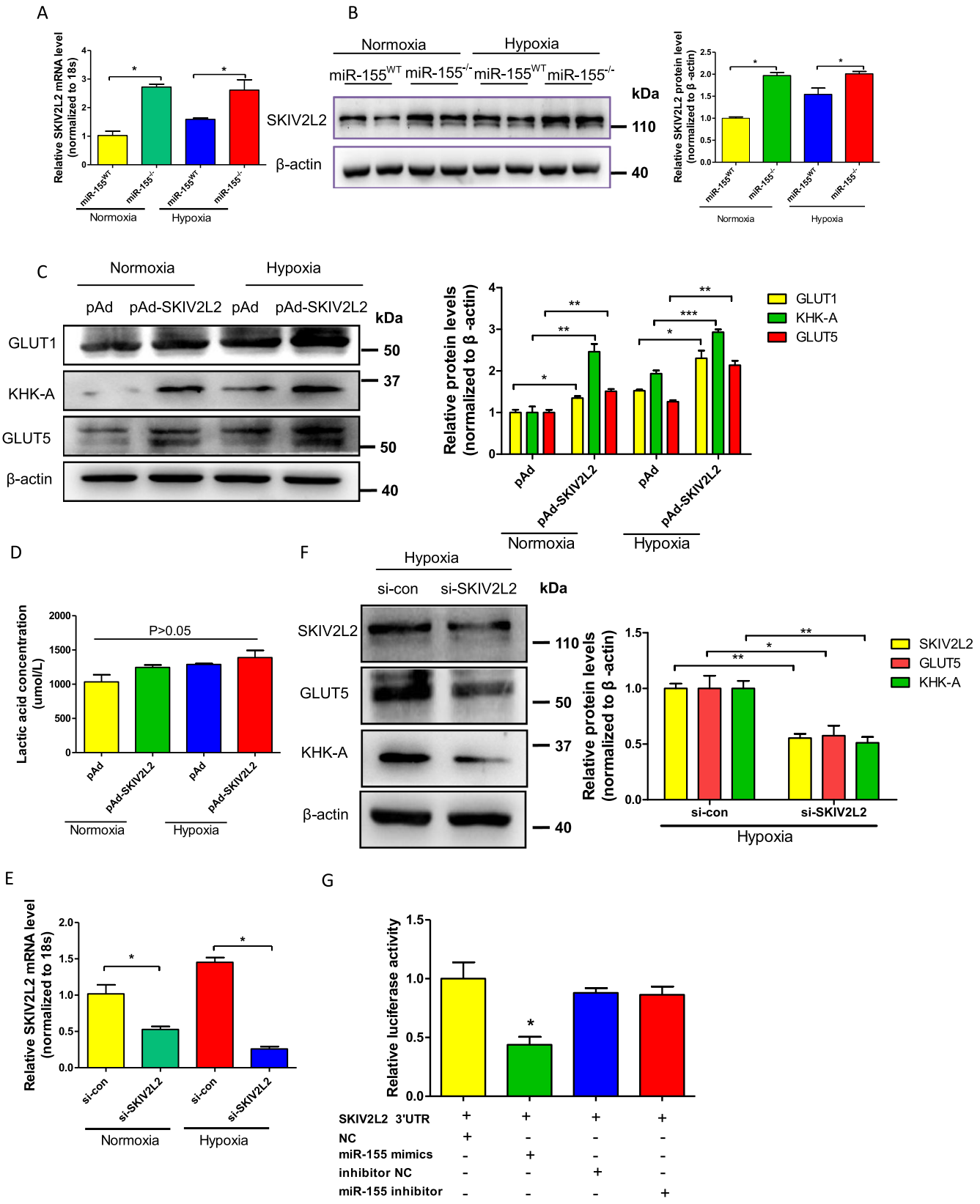
A
Relative SKIV2L2 mRNA level (normalized to 18s)
miR-155WT
miR-155-/-
Normoxia
Hypoxia
B
Normoxia
Hypoxia
miR-155WT miR-155-/- miR-155WT miR-155-/-
kDa
SKIV2L2
β-actin
110
40
Relative SKIV2L2 protein level (normalized to β -actin)
C
Normoxia
Hypoxia
pAd pAd-SKIV2L2 pAd pAd-SKIV2L2
kDa
GLUT1
KHK-A
GLUT5
β-actin
50
37
50
40
Relative protein levels (normalized to β -actin)
GLUT1
KHK-A
GLUT5
D
Lactic acid concentration (umol/L)
P>0.05
F
Hypoxia
si-con si-SKIV2L2
kDa
SKIV2L2
GLUT5
KHK-A
β-actin
110
50
37
40
Relative protein levels (normalized to β -actin)
SKIV2L2
GLUT5
KHK-A
E
Relative SKIV2L2 mRNA level (normalized to 18s)
si-con
si-SKIV2L2
G
Relative luciferase activity
SKIV2L2 3'UTR
NC
miR-155 mimics
inhibitor NC
miR-155 inhibitor

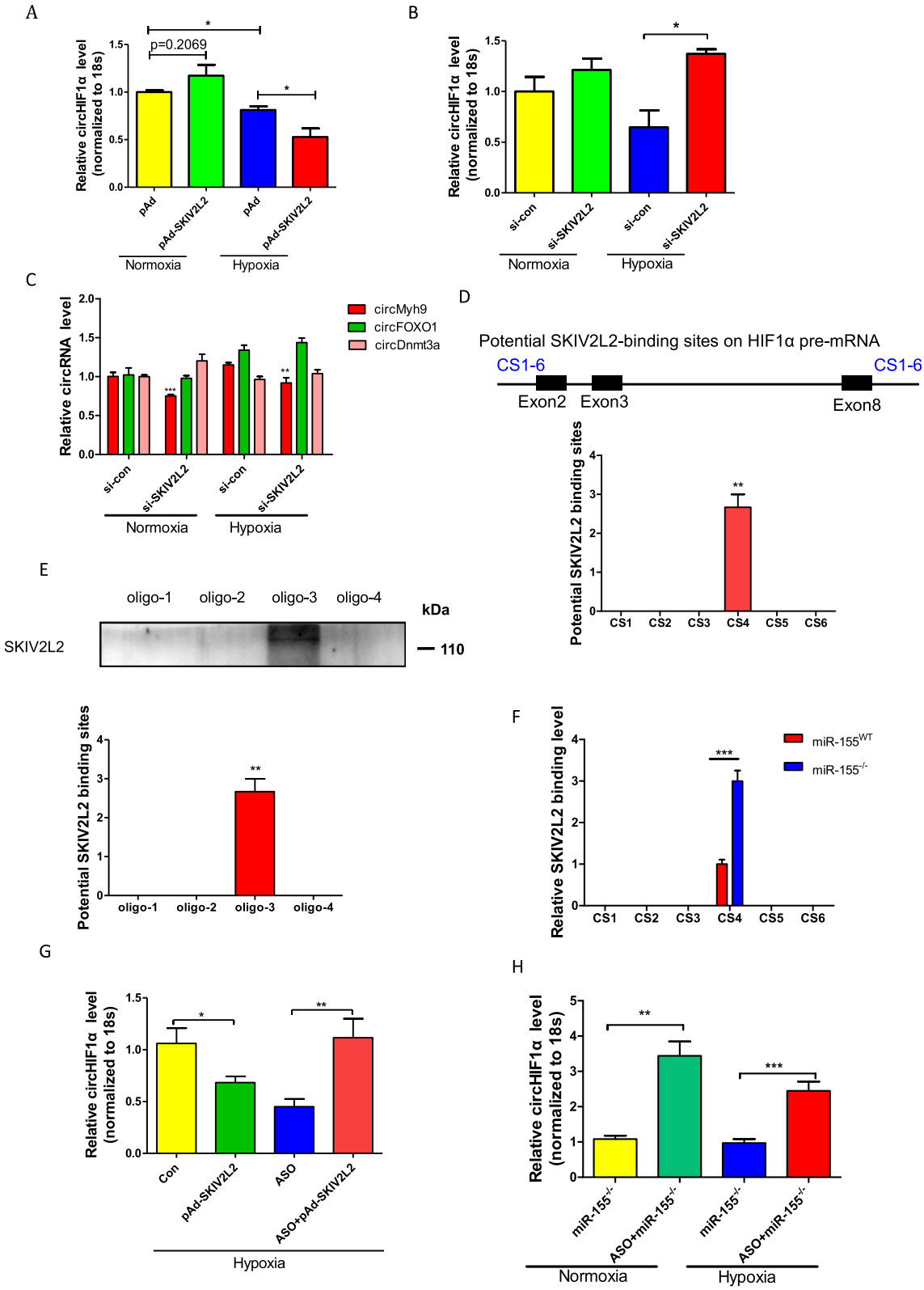
A
Relative circHIF1α level (normalized to 18s)
p=0.2069
pAd
pAd-SKIV2L2
Normoxia
Hypoxia
B
si-con
si-SKIV2L2
C
Relative circRNA level
circMyh9
circFOXO1
circDnmt3a
D
Potential SKIV2L2-binding sites on HIF1α pre-mRNA
CS1-6
Exon2
Exon3
Exon8
Potential SKIV2L2 binding sites
CS1
CS2
CS3
CS4
CS5
CS6
E
oligo-1
oligo-2
oligo-3
oligo-4
kDa
SKIV2L2
110
F
Relative SKIV2L2 binding level
miR-155WT
miR-155-/-
G
Con
ASO
ASO+pAd-SKIV2L2
H
miR-155-/-
ASO+miR-155-/-

Fig. 4. SKIV2L2 mediates miR-155 regulation of circHIF1α expression. (A) CFs were transfected with pAd-SKIV2L2 and then exposed to normoxia or hypoxia for 24 h. circHIF1α expression was detected by qRT-PCR. *P < 0.05 vs. their corresponding control. (B) CFs were transfected with si-SKIV2L2 and then exposed to normoxia or hypoxia for 24 h. circHIF1α expression was detected by qRT-PCR. *P < 0.05 vs. si-con + hypoxia. (C) circMyh9, circFOXO1 and circDnmt3a expression in CFs treated as in (B) was detected by qRT-PCR. **P < 0.01 and ***P < 0.001 vs. si-con. (D) A schematic of HIF1α exons 2 through 8 (top). CF lysates were immunoprecipitated with anti-SKIV2L2, and the immunoprecipitates were detected by qRT-PCR with primers specific for the CS1-6 sequences (bottom). **P < 0.01. (E) An oligo pull-down assay was done with CF lysates and biotinylated double-stranded oligonucleotide (∼150 nt) surrounding and in the CS4 of HIF1α pre-mRNA. The oligo-bound protein was detected by Western blot with anti-SKIV2L2 antibody.**P < 0.01.(F) qRT-PCR detected the enrichment of the CS4 fragment by anti-SKIV2L2 in miR-155$^{-/-}$ and miR-155^{wt} CFs. ***P < 0.001 vs. miR-155^{wt} (G) CFs were transfected with the ASO of the CS4 and pAd-SKIV2L2 for 24 h. circHIF1α expression was detected by qRT-PCR. *P < 0.05 vs. Con, **P < 0.01 vs. ASO. (H) miR-155$^{-/-}$ CFs were transfected with with the ASO of the CS4 and then exposed to normoxia or hypoxia for 24 h. circHIF1α expression was detected by qRT-PCR, **P < 0.01 and ***P < 0.001 vs. miR-155$^{-/-}$. Data shown in (A)-(H) are mean ± SEM, n = 3 independent experiments.

knockdown on other circRNA expression. As shown in Fig. 4C, knockdown of SKIV2L2 did not affect the biogenesis of circFOXO1 and circDnmt3a, but decreased the expression of circMyh9, suggesting that SKIV2L2-induced formation of circRNA is specific for circHIF1α. Considering that exon cyclization can be facilitated by complementary sequences in opposite directions of RNA pairing across flanking introns and protein factors that are able to bind flanking introns and ligate unfavorable reverse splice sites into a close proximity [31], we hypothesized that SKIV2L2 might directly bind to flanking intronic *cis*-complementary sequences and stabilize RNA pairing to promote exon circularization. We thus analyzed the *cis*-complementary sequences in the intron upstream of exon 2 and downstream of exon 8 of HIF1α gene and predicted potential binding sites of SKIV2L2 on HIF1α pre-mRNA (Fig. 4D). Further, RNA-binding protein immunoprecipitation (RIP) assays were performed with antibody against SKIV2L2 and the primers shown in Supplemental Table S2 to detect the binding sites of SKIV2L2 on HIF1α pre-mRNA. The results showed that SKIV2L2 could bind to the fourth part of the *cis*-complementary sequences (CS4) (Fig. 4D). Since 1 kb long RNA fragments may bind with many proteins, we made a series of smaller (∼150 nt) RNA decoys (oligo-1, 2, 3 and 4) around CS4 of the HIF1α pre-mRNA to more specifically identify the binding site of SKIV2L2. We observed that the oligo-3 fragment could bind to SKIV2L2, whereas the oligos 1, 2 and 4 could not (Fig. 4E). These findings imply that SKIV2L2 acts as a component of the splicing factor complex to direct HIF1α pre-mRNA splicing.

Further experiments revealed that miR-155$^{-/-}$ CFs exhibited a significantly increased binding of SKIV2L2 to the CS4 compared with miR-155^{wt} CFs (Fig. 4F). To further verify this, we transfected CFs with antisense oligonucletoide (ASO) specific for the CS4 (CS4-ASO) and detected the expression of circHIF1α. As shown in Fig. 4G, the CS4-ASO attenuated circHIFa formation probably through blocking binding of SKIV2L2 to the CS4, whereas SKIV2L2 overexpression mediated by pAd-SKIV2L2 abolished the suppressive effect of the CS4-ASO on the circularization of the exon 2 and 8 of HIF1α gene. Furthermore, miR-155 deficiency in CFs could also abrogate the inhibitory effects of the CS4-ASO on circHIFa formation (Fig. 4H). Overall, our results clearly indicated that circularization of the exon 2 and 8 of HIF1α gene is induced by SKIV2L2 binding to the CS4 of HIF1α pre-mRNA.

SKIV2L2 mediates miR-155 regulation of circHIF1α expression by interacting with TRA2A

It is well known that hypoxia induces HIF-1α expression [32], and that formation of circRNA can affect its parental gene expression [33]. Next, we sought to explore the relationship between circHIF1α formation and its parent linear RNA. Firstly, we examined the effect of hypoxia on SKIV2L2 expression and found that exposure of CFs to hypoxia for 24 h significantly increased SKIV2L2 mRNA (Fig. 5A) and protein levels (Fig. 5B). Intriguingly, siRNA-mediated knockdown of SKIV2L2 in CFs upregulated HIF1α mRNA and protein expression under normoxia, but downregulated its mRNA and protein levels in hypoxia-exposed CFs (Fig. 5C, D). These findings prompted us to study whether SKIV2L2 plays different roles in the regulation of HIF1α expression under normoxia and hypoxia conditions by interacting with different protein factors. We therefore performed a mass spectrometry analysis of the complexes precipitated with antibody against SKIV2L2. As shown in Fig. 5E, 250 proteins were identified to be differentially expressed in normoxia vs. hypoxia. Among them, only 3 proteins have been reported to be involved in splicing regulation. We here focused on TRA2A, which mediates alternative mRNA splicing [34], and investigated whether TRA2A is indeed able to influence alternative pre-mRNA splicing. Co-IP assays revealed that the interaction between TRA2A and SKIV2L2 was apparently strengthened in hypoxia-exposed miR-155^{wt} and miR-155$^{-/-}$ CFs although miR-155 deletion in CFs slightly attenuated the association of TRA2A with SKIV2L2 compared with miR-155^{wt} CFs (Fig. 5F). Furthermore, knockdown of TRA2A (Supplemental data, SFig.3C) increased the expression of circHIF1α regardless of hypoxia treatment (Fig. 5G, left panel) but did not significantly affect HIF1α mRNA expression level (Fig. 5G, right panel), suggesting that miR-155 deletion in CFs reduces circHIF1α expression via facilitating the association of TRA2A with SKIV2L2.

Exogenous delivery of SKIV2L2 has a protective effect on the infarcted heart

To address the translational implications of the SKIV2L2 in ischemic heart disease, we investigated whether manipulating SKIV2L2 expression can provide a protective effect on the infarcted

Fig. 5. SKIV2L2 mediates miR-155 regulation of circHIF1α expression by interacting with TRA2A. (A) SKIV2L2 mRNA expression in CFs exposed to hypoxia or normoxia for 24 h was detected by qRT-PCR. *P < 0.05 vs. normoxia (*n* = 3 independent experiments). (B) SKIV2L2 expression in CFs treated as in (A) was detected by Western blot. Representative images (left) and semi-quantitative chart (right). **P < 0.01 vs. normoxia (n = 3 independent experiments). (C) CFs were transfected with si-SKIV2L2 and then exposed to normoxia or hypoxia for 24 h. HIF1α mRNA was detected by qRT-PCR. *P < 0.05 and ***P < 0.001 vs. si-con (*n* = 4 independent experiments). (D) HIF1α expression in SKIV2L2$^{-/-}$ and SKIV2L2 CFs exposed to normoxia or hypoxia for 24 h was detected by Western blot. Representative images (left) and semi-quantitative chart (right). *P < 0.05 and ***P < 0.001 vs. SKIV2L2. (E) Mass spectrometry analysis detected TRA2A in anti-SKIV2L2 immunoprecipitates (n = 3 independent experiments). (F) The lysates of miR-155$^{-/-}$ and miR-155^{wt} CFs were immunoprecipitated with anti-TRA2A. SKIV2L2 in the immunoprecipitates was measured by Western blotting. Representative images (upper) and semi-quantitative chart (lower), ***P < 0.001 vs. miR-155^{wt} + Normoxia, $^{\#\#}$P < 0.01 vs. miR-155$^{-/-}$ + Normoxia (n = 3 independent experiments). (G) CFs were transfected with si-TRA2A and then exposed to normoxia or hypoxia for 24 h. circHIF1α and HIF1α mRNA expression was detected by qRT-PCR. *P < 0.05 vs. si-con (n = 3 independent experiments).

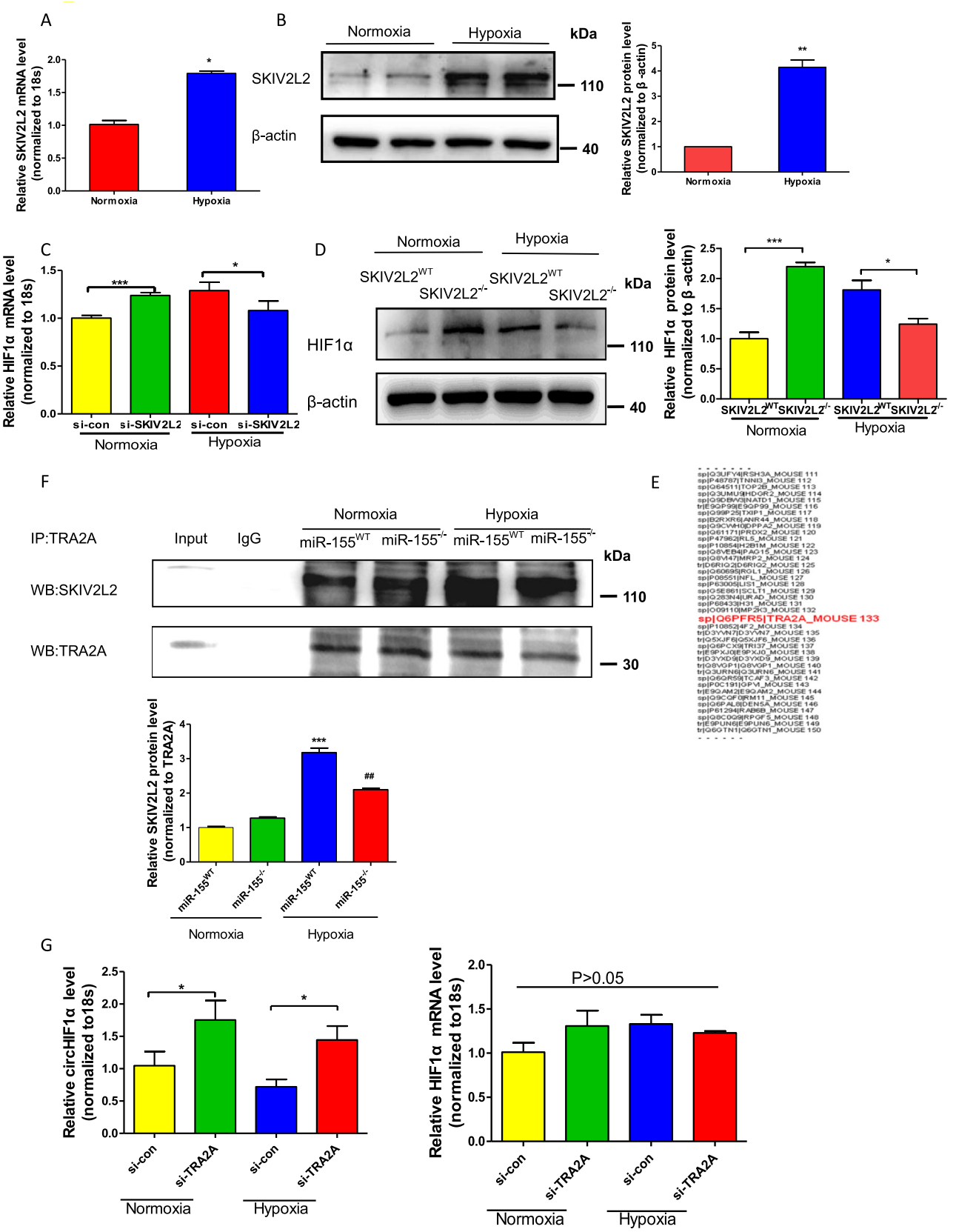
A
Relative SKIV2L2 mRNA level (normalized to 18s)
Normoxia
Hypoxia
B
Normoxia
Hypoxia
kDa
SKIV2L2
β-actin
110
40
Relative SKIV2L2 protein level (normalized to β -actin)
C
Relative HIF1α mRNA level (normalized to 18s)
si-con
si-SKIV2L2
D
SKIV2L2WT
SKIV2L2-/-
HIF1α
Relative HIF1α protein level (normalized to β -actin)
E
sp|Q6PFR5|TRA2A_MOUSE 133
F
IP:TRA2A
Input
IgG
miR-155WT
miR-155-/-
WB:SKIV2L2
WB:TRA2A
30
Relative SKIV2L2 protein level (normalized to TRA2A)
G
Relative circHIF1α level (normalized to18s)
si-TRA2A
Relative HIF1α mRNA level (normalized to18s)
P>0.05

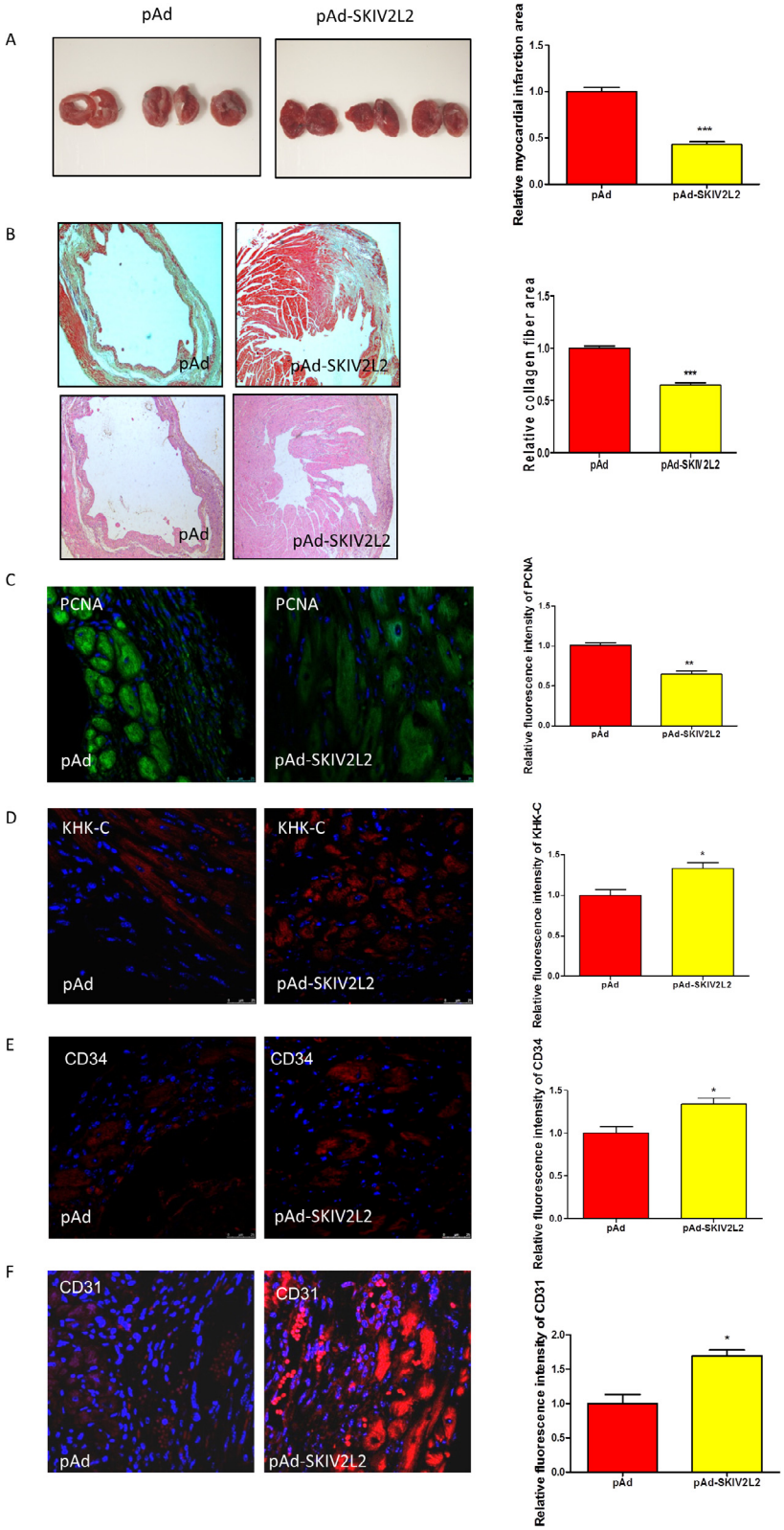

Fig. 6. Exogenous delivery of SKIV2L2 has a protective effect on the infarcted heart. (A) The infarct area of pAd and pAd-SKIV2L2-transduced mouse heart was detected by TTC staining at 14 days after MI. ***P < 0.001 vs. pAd. (B) Hematoxylin-eosin (bottom) and Masson trichrome staining (top) of the cardiac tissue harvested at 2 weeks after MI in control and pAd-SKIV2L2-transduced mice. ***P < 0.001 vs. pAd. (C-F) Immunofluorescence staining of PCNA (C, green), KHK-C (D, red), CD34 (E, red) and CD31 (F, red) in pAd and pAd-SKIV2L2-transduced mouse cardiac tissue. Representative images (left) and semi-quantitative chart (right). Data are presented as mean ± SEM from a minimum of 3 independent experiments (n = 5 mice/group). *P < 0.05 and **P < 0.01 vs. pAd.

heart. We therefore established an acute myocardial infarction (MI) model in mice by ligation of the left anterior descending branch of the coronary artery, and pAd-SKIV2L2 was intramyocardially injected immediately after coronary artery ligation. Negative control mice received no treatment after MI. TTC staining was performed at 14 days after MI to measure the infarct area. As shown in

Fig. 6A, the infarct area was largely reduced in SKIV2L2-transduced heart. Left ventricle morphometry imaged by Masson's trichrome staining revealed that enforced expression of SKIV2L2 in myocardial tissues significantly decreased collagen accumulation, indicating a protective effect of SKIV2L2 on the infarcted heart (Fig. 6B). To reveal the mechanisms underlying the protective effect of SKIV2L2, we investigated whether the enforced expression of SKIV2L is able to activate fructose metabolism and improve cell survival in the infarcted heart. Immunofluorescence staining for PCNA, KHK-C, CD34, and CD31 showed that SKIV2L2-transduced hearts exhibited an increased expression of KHK-C, CD34 and CD31, with a concomitant decline in PCNA expression (Fig. 6C–F). We also found that the tube formation ability of endothelial cells, such as the number and the length of the tubes, was significantly increased in SKIV2L2-overexpressing cells (SFig.4). The increase in CD31 expression and the tube formation indicated that angiogenesis is improved by overexpression of SKIV2L2. Altogether, these results suggest that increased expression of SKIV2L2 by exogenous gene transfer may exert a protective effect on the infarcted heart through activating fructose metabolism and promoting angiogenesis.

Discussion

Metabolic disturbances contribute to the development of a number of diseases, such as diabetes, obesity, cancer, and cardiovascular diseases. On the other hand, in response to chronic pathologic stress, pathophysiological changes that occur in different tissues and organs lead to the production of some growth signals and tissue hypoxia, which directs the cell to reprogram its metabolism to support energy homeostasis [35]. In the cardiovascular system, myocardial ischemia-induced glycolysis, referred to as the Warburg effect, has been shown to be activated in many disease-relevant cell types, including smooth muscle cells (SMC), endothelial cells (EC), cardiac fibroblasts (CFs) and ventricle cardiomyocytes [35]. In the present study, we found that both miR-155$^{-/-}$ and miR-155^{wt} CFs exposed to hypoxia exhibited an increased glycolysis, but only in miR-155$^{-/-}$ CFs exposed to hypoxia, the expression of ketohexokinase (KHK)-A and KHK-C was significantly upregulated, implying that fructose metabolism is actuated. These suggest that miR-155 downregulation in hypoxia-exposed CFs is responsible for the activation of fructose metabolism. Mechanistically, we showed that miR-155 deletion in CFs exposed to hypoxia enhanced SKIV2L2 expression and its interaction with TRA2A, which in turn suppresses alternative splicing of HIF1α pre-mRNA to form circHIF1α, and then decreased circHIF1α contributes to the activation of fructose metabolism through inducing production of the KHK-C isoform. In this study, we provided a novel insight into the functional significance of fructolysis in hypoxia-exposed CFs.

In this study, there exist some differences between the protein and mRNA levels of GLUT1 under normoxia condition. Our results showed that the expression level of GLUT1 protein was substantially decreased in normoxia-treated miR-155$^{-/-}$ CFs compared with that in normoxia-treated miR-155^{wt} CFs, whereas its mRNA expression did not reveal significant difference between these two cells under the same condition. We speculated that miR-155 deficiency in CFs could probably induce a currently unknown binding partner, which facilitates GLUT1 ubiquitination and the subsequent degradation. However, the excise mechanisms whereby GLUT1 protein stability is regulated by miR-155 need to be further elucidated.

The key enzyme for fructose metabolism is ketohexokinase (KHK) [36]. KHK has two different isoforms, KHK-A and KHK-C [37,38]. Among them, the KHK-C isoform has a very high affinity for fructose, which is beneficial to fructose metabolism [39]. This enzyme catalyzes the conversion of fructose to fructose-1-phosphate (F-1-P). Therefore, the decomposition reaction of fructose can bypass the rate-limiting step of the glycolysis pathway to directly generate fructose 1,6-diphosphate and then enter the glycolysis pathway. Thus, bypassing the rate-limiting step of the glycolysis pathway may make cardiomyocytes more sensitive to changes in energy requirements, increasing glycolysis flux to meet the energy needs of the myocardium to maintain cardiac contractility. However, if the hypoxic environment is not relieved for a long time, increased glucose metabolism is not sufficient to compensate for the energy loss of fatty acid oxidation, fructose metabolism will be actuated to compensate for the lack of energy, which will eventually cause myocardial pathological hypertrophy and heart failure.

Given the fact that miR-155$^{-/-}$ mice has a stronger anti-hypoxia ability than miR-155^{wt} mice, we therefore speculated that, in order to adapt to the hypoxic survival environment caused by myocardial hypoxia, miR-155$^{-/-}$ cardiomyocytes undergo metabolic remodeling and a switch to fructose metabolism mediated by KHK-C. How does miR-155 deletion in CFs affect glucose metabolism under hypoxia? In recent years, circRNA, as a star molecule, has led to many research fields to make important breakthroughs. Our microarray analysis of circRNAs in miR-155$^{-/-}$ vs. miR-155^{wt} CFs exposed to hypoxia showed that circHIF1α expression level was significantly different between these two cells. It is well known that HIF1α is the core transcription factor of the body's response to low oxygen tension [40]. Under pathologic stress, HIF1α, as a regulator of the alternative splicing machinery, transcriptionally activates a number of splicing factors, including SF3B1. SF3B1 leads to the production of the KHK-C isoform by binding to the branch point in front of the KHK 3c exon [4]. However, it is still unclear (1) Is the circHIF1α generated by alternative splicing in hypoxia-exposed CFs? (2) How does miR-155 regulate the formation of circHIF1α? (3) How does circHIF1α regulate metabolic remodeling in hypoxia-exposed CFs? (4) Which splicing factors participate in the alternative splicing of HIF1α pre-mRNA? To answer these questions, we constructed the expression vector of circHIF1α and demonstrated that overexpression of circHIF1α inhibited the migration of CFs induced by hypoxia and decreased GLUT5 mRNA and protein expression as well as KHK-C protein level under hypoxia. Under normoxia, however, its overexpression significantly increased the expression levels of GLUT5, KHK-A and KHK-C. More importantly, combining circHIF1α overexpression with miR-155 silencing enhanced the expression of fructose-metabolizing enzymes KHK-A and KHK-C in hypoxia-exposed CFs, accompanied by a transcriptional induction of the fructose-specific transporter GLUT5. These suggest that decreased expression of circHIF1α by miR-155 downregulation contributes to the activation of fructose metabolism through inducing GLUT5 expression and the production of the KHK-C isoform.

To further investigate how miR-155 deletion affects circHIF1α formation under hypoxic conditions, we screened the splicing-associated proteins differentially expressed in miR-155$^{-/-}$ vs. miR-155^{wt} CFs exposed to hypoxia. The results showed that knockout of miR-155 in CFs could significantly upregulate the expression of SKIV2L2, also named as MTR4. The biochemical role of SKIV2L2, as an RNA helicase in RNA processing, has been extensively studied, but its role in alternative splicing is still poorly understood. Yu L et al. found that MTR4 facilitates liver tumorigenesis by promoting cancer metabolic conversion through alternative splicing [41]. Consistent with their results, our findings reveal that SKIV2L2 also played an important role in regulating alternative splicing associated with metabolic remodeling in hypoxia-exposed CFs, identifying a novel role of SKIV2L2 in CFs. Considering that circRNAs exert their functions generally through the regulation of

their target genes and miRNAs, we speculated that there may be an intermediate that is negatively regulated by miR-155 and transmits its signal to drive changes in the expression of metabolic genes. Since the SKIV2L2 is known to participate in circRNA biogenesis and we found that circHIF1α was differentially expressed in miR-155$^{-/-}$ vs. miR-155^{wt} CFs, we selected SKIV2L2 as such a mediator candidate for further investigation. Indeed, we found that SKIV2L2 expression was dramatically upregulated in miR-155$^{-/-}$ CFs, suggesting that the ratio of circHIF1α and HIF1α mRNA is probably regulated by SKIV2L2, and that the ratio change between them may be related to hypoxia-induced metabolic remodeling. To further determine whether other factors are also involved in the regulation of circHIF1α/HIF1α mRNA balance, RIP and mass spectrometry analysis were performed and identified TRA2A, a known splicing factor, as an important splicing factor that can enhance HIF1α pre-mRNA alternative splicing under hypoxia. Based on the experimental results of Mirtschink et al [4] and our observations, we reasonably speculate that in hypoxia-exposed myocardial tissues, miR-155 can couple a series of molecular and cellular biological events including alternative splicing of HIF1α pre-mRNA and myocardial metabolic remodeling.

It is worth noting that the heart contains various types of cells, including cardiomyocytes, CFs, many kinds of immune cells and vascular cells. Among these cells, cardiomyocytes directly reflect the contractile function of the heart, whereas CFs play pivotal functions in the maintenance of cardiac function, physiological cardiac remodeling after heart stress and pathological remodeling [42]. Although it is possible that the pathological crosstalk exists between cardiomyocytes and CFs under stress condition, their crosstalk pathways and the underlying mechanisms remain to be clarified. Based on our existing knowledge, we reasonably speculate that (1) CFs regulate cardiomyocyte metabolism and function in a paracrine manner through releasing bioactive factors; (2) exosomes secreted by CFs exert the regulatory effects on the cardiomyocytes. The activation of fructose metabolism in hypoxic CFs by miR-155 downregulation can alter the secretion of bioactive factors and exosomes, thus protecting the cardiomyocytes from the damage mediated by hypoxic CFs. However, the precise mechanisms underlying cardiomyocyte protection by the activation of fructose metabolism from the hypoxia damage need to be addressed in future studies.

Conclusion

Deficiency of miR-155 in CFs can significantly upregulate the expression of SKIV2L2 which plays an important role in regulating alternative splicing of HIF1α pre-mRNA by interacting with TRA2A. Our findings indicated that increased SKIV2L2 facilitates GLUT5 and KHK-C expression through inducing circHIF1α formation, which in turn actuates fructose metabolism. Our results also suggested that increased expression of SKIV2L2 by exogenous gene transfer may exert a protective effect on the infarcted heart through activating fructose metabolism and promoting angiogenesis, thus providing a new research direction for the mechanisms of occurrence and development of hypoxia-related cardiovascular diseases.

Ethics statement

All procedures involving experimental animals were performed in accordance with the principles and guidelines established by the National Institute of Medical Research (INSERM) and were approved by the local Animal Care and Use Committee. The investigation conforms to the directive 2010/63/EU of the European parliament.

Declaration of Competing Interest

We declare no conflicts of interest (both financial and personal). I affirm that the manuscript has not been published previously and is not being considered concurrently for publication elsewhere. All authors and acknowledged contributors have read and approved the manuscript.

Acknowledgements

This study was supported by the National Natural Science Foundation of China (No. 81971328; NO.81770285; NO.31871152), Key R & D projects of Hebei Province (19277762D), Key research projects of science and technology in universities of Hebei Province (ZD2019100), Scientific research project of high level talents in universities of Hebei Province (GCC2014026). Scientific and technology Research Foundation for Colleges and universities of Hebei Province (QN2017102).

Appendix A. Supplementary material

Supplementary data to this article can be found online at https://doi.org/10.1016/j.jare.2021.10.007.

References

[1] Stanley WC, Chandler MP. Energy metabolism in the normal and failing heart: potential for therapeutic interventions. Heart Fail Rev 2002;7(2):115–30.
[2] Mirtschink P, Krek W. Hypoxia-driven glycolytic and fructolytic metabolic programs: Pivotal to hypertrophic heart disease. Biochim Biophys Acta 2016;1863(7):1822–8.
[3] Kaelin WG, Ratcliffe PJ. Oxygen sensing by metazoans: the central role of the HIF hydroxylase pathway. Mol Cell 2008;30(4):393–402.
[4] Mirtschink P, Krishnan J, Grimm F, Sarre A, Hörl M, Kayikci M, et al. HIF-driven SF3B1 induces KHK-C to enforce fructolysis and heart disease. Nature 2015;522(7557):444–9.
[5] Yang Z, Zheng B, Zhang Y, He M, Zhang X-H, Ma D, et al. miR-155-dependent regulation of mammalian sterile 20-like kinase 2 (MST2) coordinates inflammation, oxidative stress and proliferation in vascular smooth muscle cells. Biochim Biophys Acta 2015;1852(7):1477–89.
[6] Tian FJ, An LN, Wang GK, Zhu JQ, Li Q, Zhang YY, et al. Elevated microRNA-155 promotes foam cell formation by targeting HBP1 in atherogenesis. Cardiovasc Res 2014;103(1):100–10.
[7] Shen G, Li X, Jia Y-F, Piazza GA, Xi Y. Hypoxia-regulated microRNAs in human cancer. Acta Pharmacol Sin 2013;34(3):336–41.
[8] Bruning U, Cerone L, Neufeld Z, Fitzpatrick SF, Cheong A, Scholz CC, et al. MicroRNA-155 promotes resolution of hypoxia-inducible factor 1alpha activity during prolonged hypoxia. Mol Cell Biol 2011;31(19):4087–96.
[9] Zhang RN, Zheng B, Li LM, Zhang J, Zhang XH, Wen JK. Tongxinluo inhibits vascular inflammation and neointimal hyperplasia through blockade of the positive feedback loop between miR-155 and TNF-alpha. Am J Physiol Heart Circ Physiol 2014;307(4):H552–62.
[10] Krishnan J, Suter M, Windak R, Krebs T, Felley A, Montessuit C, et al. Activation of a HIF1alpha-PPARgamma axis underlies the integration of glycolytic and lipid anabolic pathways in pathologic cardiac hypertrophy. Cell Metab 2009;9(6):512–24.
[11] Zhang M-l, Zheng B, Tong F, Yang Z, Wang Z-b, Yang B-M, et al. iNOS-derived peroxynitrite mediates high glucose-induced inflammatory gene expression in vascular smooth muscle cells through promoting KLF5 expression and nitration. Biochim Biophys Acta Mol Basis Dis 2017;1863(11):2821–34.
[12] Wu J, Subbaiah KCV, Xie LH, Jiang F, Khor E-S, Mickelsen D, et al. Glutamyl-prolyl-tRNA synthetase regulates proline-rich pro-fibrotic protein synthesis during cardiac fibrosis. Circ Res 2020;127(6):827–46.
[13] Zhang Yu, Li YH, Liu C, Nie C-J, Zhang X-H, Zheng C-Y, et al. miR-29a regulates vascular neointimal hyperplasia by targeting YY1. Cell Prolif 2017;50(3):e12322. doi: https://doi.org/10.1111/cpr.2017.50.issue-310.1111/cpr.12322.
[14] Song H-F, He S, Li S-H, Wu J, Yin W, Shao Z, et al. Knock-out of MicroRNA 145 impairs cardiac fibroblast function and wound healing post-myocardial infarction. J Cell Mol Med 2020;24(16):9409–19.
[15] Ma D, Zheng B, Liu H-L, Zhao Y-b, Liu X, Zhang X-H, et al. Klf5 down-regulation induces vascular senescence through eIF5a depletion and mitochondrial fission. PLoS Biol 2020;18(8):e3000808.
[16] Xia H, Chen J, Gao H, Kong SN, Deivasigamani A, Shi M, et al. Hypoxia-induced modulation of glucose transporter expression impacts (18)F-fluorodeoxyglucose PET-CT imaging in hepatocellular carcinoma. Eur J Nucl Med Mol Imaging 2020;47(4):787–97.

[17] Xu BH, Sheng J, You YK, Huang XR, Ma RCW, Wang Q, et al. Deletion of Smad3 prevents renal fibrosis and inflammation in type 2 diabetic nephropathy. Metabol: Clin Exp 2020;103:154013.
[18] Yang Z, Qu C-B, Zhang Y, Zhang W-F, Wang D-D, Gao C-C, et al. Dysregulation of p53-RBM25-mediated circAMOTL1L biogenesis contributes to prostate cancer progression through the circAMOTL1L-miR-193a-5p-Pcdha pathway. Oncogene 2019;38(14):2516–32.
[19] Can E, Mishkovsky M, Yoshihara HAI, Kunz N, Couturier D-L, Petrausch U, et al. Noninvasive rapid detection of metabolic adaptation in activated human T lymphocytes by hyperpolarized (13)C magnetic resonance. Sci Rep 2020;10 (1):200.
[20] Faraoni I, Antonetti FR, Cardone J, Bonmassar E. miR-155 gene: a typical multifunctional microRNA. Biochim Biophys Acta 2009;1792(6):497–505.
[21] Marques-Rocha JL, Samblas M, Milagro FI, Bressan J, Martínez JA, Marti A. Noncoding RNAs, cytokines, and inflammation-related diseases. FASEB J 2015;29(9):3595–611.
[22] Semba H, Takeda N, Isagawa T, Sugiura Y, Honda K, Wake M, et al. HIF-1alpha-PDK1 axis-induced active glycolysis plays an essential role in macrophage migratory capacity. Nat Commun 2016;7:11635.
[23] Peng F, Wang JH, Fan WJ, Meng YT, Li MM, Li TT, et al. Glycolysis gatekeeper PDK1 reprograms breast cancer stem cells under hypoxia. Oncogene 2018;37 (8):1119.
[24] Wang JZ, Zhu W, Han J, Yang X, Zhou R, Lu HC, et al. The role of the HIF-1alpha/ALYREF/PKM2 axis in glycolysis and tumorigenesis of bladder cancer. Cancer Commun (Lond, England) 2021;41(7):560–75.
[25] Moon J-S, Lee S, Park M-A, Siempos II, Haslip M, Lee PJ, et al. UCP2-induced fatty acid synthase promotes NLRP3 inflammasome activation during sepsis. J Clin Invest 2015;125(2):665–80.
[26] Geisler CE, Ghimire S, Bogan RL, Renquist BJ. Role of ketone signaling in the hepatic response to fasting. Am J Physiol Gastrointest Liver Physiol 2019;316 (5):G623–31.
[27] He A, Chen X, Tan M, Chen Y, Lu D, Zhang X, et al. Acetyl-CoA Derived from Hepatic Peroxisomal beta-Oxidation Inhibits Autophagy and Promotes Steatosis via mTORC1 Activation. Mol Cell 2020;79(1):30–42-e34.
[28] Li J, Huang Q, Long X, Zhang J, Huang X, Aa J, et al. CD147 reprograms fatty acid metabolism in hepatocellular carcinoma cells through Akt/mTOR/SREBP1c and P38/PPARalpha pathways. J Hepatol 2015;63(6):1378–89.
[29] Wu X, Li J, Yang X, Bai X, Shi J, Gao J, et al. miR-155 inhibits the formation of hypertrophic scar fibroblasts by targeting HIF-1alpha via PI3K/AKT pathway. J Mol Histol 2018;49(4):377–87.
[30] Onderak AM, Anderson JT. Loss of the RNA helicase SKIV2L2 impairs mitotic progression and replication-dependent histone mRNA turnover in murine cell lines. RNA 2017;23(6):910–26.
[31] Dong R, Ma X-K, Chen L-L, Yang Li. Increased complexity of circRNA expression during species evolution. RNA Biol 2017;14(8):1064–74.
[32] Wang GL, Jiang BH, Rue EA, Semenza GL. Hypoxia-inducible factor 1 is a basic-helix-loop-helix-PAS heterodimer regulated by cellular O2 tension. Proc Natl Acad Sci U S A 1995;92(12):5510–4.
[33] Zhao X, Cai Y, Xu J. Circular RNAs: Biogenesis, Mechanism, and Function in Human Cancers. Int J Mol Sci 2019;20(16).
[34] Zhu Y, Wang R, Yu L, Sun H, Tian S, Li P, et al. Human TRA2A determines influenza A virus host adaptation by regulating viral mRNA splicing. Sci Adv 2020;6(25):aaz5764.
[35] Tian L, Wu D, Dasgupta A, Chen K-H, Mewburn J, Potus F, et al. Epigenetic Metabolic Reprogramming of Right Ventricular Fibroblasts in Pulmonary Arterial Hypertension: A Pyruvate Dehydrogenase Kinase-Dependent Shift in Mitochondrial Metabolism Promotes Right Ventricular Fibrosis. Circ Res 2020;126(12):1723–45.
[36] Kim J, Kang J, Kang Y-L, Woo J, Kim Y, Huh J, et al. Ketohexokinase-A acts as a nuclear protein kinase that mediates fructose-induced metastasis in breast cancer. Nat Commun 2020;11(1). doi: https://doi.org/10.1038/s41467-020-19263-1.
[37] Li X, Qian X, Peng LX, Jiang Y, Hawke DH, Zheng Y, et al. A splicing switch from ketohexokinase-C to ketohexokinase-A drives hepatocellular carcinoma formation. Nat Cell Biol 2016;18(5):561–71.
[38] Doke T, Ishimoto T, Hayasaki T, Ikeda S, Hasebe M, Hirayama A, et al. Lacking ketohexokinase-A exacerbates renal injury in streptozotocin-induced diabetic mice. Metab Clin Exp 2018;85:161–70.
[39] Lanaspa MA, Andres-Hernando A, Orlicky DJ, Cicerchi C, Jang C, Li N, et al. Ketohexokinase C blockade ameliorates fructose-induced metabolic dysfunction in fructose-sensitive mice. J Clin Invest 2018;128(6):2226–38.
[40] Sun W, Wang B, Qu X-L, Zheng B-Q, Huang W-D, Sun Z-W, et al. Metabolism of Reactive Oxygen Species in Osteosarcoma and Potential Treatment Applications. Cells 2019;9(1):87. doi: https://doi.org/10.3390/cells9010087.
[41] Yu L, Kim J, Jiang L, Feng B, Ying Y, Ji K-Y, et al. MTR4 drives liver tumorigenesis by promoting cancer metabolic switch through alternative splicing. Nat Commun 2020;11(1). doi: https://doi.org/10.1038/s41467-020-14437-3.
[42] Fujiu K, Nagai R. Contributions of cardiomyocyte-cardiac fibroblast-immune cell interactions in heart failure development. Basic Res Cardiol 2013;108 (4):357.